The effect of anisotropic microtubule-bound nucleations on ordering in the plant cortical array.

Panayiotis Foteinopoulos and Bela M. Mulder (mulder@amolf.nl)
Department of Systems Biophysics, FOM Institute AMOLF, Science Park 104, 1098XG Amsterdam, the Netherlands

Abstract. The highly orientationally ordered cortical microtubule array in plant cells is a key component for cell growth and development. Recent experimental and computational work has shown that the anisotropic nucleation of new microtubules from pre-existing microtubules has a major effect on the alignment process. We formulate a theoretical model to investigate the role of the microtubule-bound nucleation on the self-organization of the dynamical cortical microtubules. A bifurcation analysis of the stability of the disordered phase of the model reveals that the effective degree of co-aligned nucleation is the main determinant of the location of the transition. Increased co-aligned nucleation creates a positive feedback effect on the ordering process that can significantly widen the ordered region. We validate these predictions by comparing to the results of particle-based simulations.

Keywords: Cytoskeleton,Microtubules,Plant Cell Biology, Analytical model, Self-organisation

1. Introduction

Microtubules are dynamic filamentous protein aggregates and a key constituent of the cytoskeleton of all eukaryotic cells. They can reach lengths of several ten's of μm's and are therefore able to span lengths comparable to the dimensions of cells. This allows them to perform a host of functions related to establishing and maintaining the morphology and mechanical properties of cells. In plants, a number of cell types, e.g. the well-studied root cells, grow by expansion along a single axis [1], and microtubules (hereafter abbreviated as MTs) play a key role in defining this axis. They do so by setting up a plant-unique structure called the transverse cortical array, a highly aligned arrangement of microtubules bound to the inside of the plasma membrane [2]. There is mounting evidence that the MTs in the transverse array guide the insertion and the direction of motion cellulose synthase complexes [3, 4]. These complexes deposit cellulose microfibrils, the main architectural component of the plant cell wall. The widely accepted idea is that the ensuing transverse orientation of the cellulose microfibrils allows the cells to elongate in a single direction, whilst maintaining mechanical integrity in the face of an appreciable internal osmotic pressure (turgor).

A crucial aspect of MTs and the structures they form is that they are both dynamic and intrinsically out of thermodynamic equilibrium. Individual MTs alternate stochastically between growing and shrinking states in an energy-consuming process dubbed "dynamic instability" [5]. In the plant cortical array, where the MTs are bound to the plasma membrane and hence form an effectively 2D system, it is this process which drives collisions between growing MTs and obstructing MTs. The stochastic and angle-of-incidence dependent outcomes of these collisions are classified as (i) *zippering*, where the incoming MT alters its course by bending and continues to grow along the obstructing MT, (ii) *induced catastrophes*, where the incoming MT rapidly switches from a growing to a shrinking state, and (iii) *cross-overs*, where the incoming MT manages to "slip over" the obstructing one and continues to grow in its original direction [6]. Several groups have shown how the ordering of the cortical array (hereafter abbreviated as CA) can be understood on the basis of these collisions, using both computer simulations [7, 8, 9] and an analytical model [10]. The dynamical instability process implies that MTs can shrink to zero length and thus are expected to have a finite lifetime. This means that in order to achieve a steady state, new MTs need to be nucleated at a finite rate, for which cells employ specific nucleation complexes called γ-TuRCS [11]. In most of the modeling approaches the nucleation of new MTs was assumed to occur homogeneously distributed over the 2D "cortex" and in arbitrary directions, as is observed during the initial stages of CA formation. In the later stages of CA formation, when there is an appreciable density of MTs, most of the nucleations actually occur from preexisting MTs, and moreover with a specific orientational distribution with respect to the direction of the parent MT [12, 13, 14].

In a previous paper [15] we have addressed the impact of this MT-bound orientationally-biased nucleation mechanism on CA ordering using computer simulations, showing among others that (partially) co-aligning the newly nucleated MTs with the parent MTs provides a positive feedback on the ordering process, significantly widening the range of parameters for which the aligned state is stable. Here we provide the theoretical underpinning of these observations by generalizing our previously developed analytical model to explicitly incorporate anisotropic microtubule-bound nucleations. This allows us to perform a full parametric analysis of the location of the ordering transition in the presence of these more complex nucleations. Significantly, this analysis reveals that the co-alignment parameter ν_2 introduced on phenomenological grounds in [15], is indeed also formally the system parameter that most strongly influences the propensity of the system to order. Moreover, the full model allows us to go beyond the simulations by

also considering the effect of different firing rates of the nucleation complexes whether in the bound- or the unbound state, and showing how this difference interacts with the effects of differential binding of the nucleation complexes to the MTs.

The outline of the paper is as follows. In Section 2 we present our theory, first recapping the basic elements of the formalism (Section 2.1), then implementing a binding equilibrium for the nucleation complexes (Section 2.2), discuss the treatment of anisotropic nucleations (Section 2.3), finishing with a dimensional analysis, which reveals a single parameter that governs the influence of the MT-bound nucleations (Section 2.4). In Section 3 we locate the critical values of the control parameter of the system using bifurcation analysis (Section 3.1), calculate the latter numerically (Section 3.2) and compare with simulations (Section 3.3). We end with conclusions and outlook in Section 4.

2. Theoretical framework

2.1. Basic theory

Here we first recap the basic elements of the analytical model by Hawkins, Tindemans and Mulder [10]) for the mechanism of orientational order of the plant CA.

The cortical MTs are confined to a 2D plane and each MT is considered to consist of one or more straight segments with a fixed orientation, connected end-to-end. The intrinsic dynamics of the MTs is described by the standard two-state dynamic instability model of Dogterom and Leibler [16], which assumes that each MT has a "plus" end on its final segment that is either growing with speed v^+ or shrinking with speed v^-. This plus end can switch stochastically from growing to shrinking, a so-called *spontaneous catastrophe*, with rate r_c, or from shrinking to growing, a so-called *rescue*, with rate r_r. The dynamics of the interactions between colliding MTs dynamics is encoded into the probabilities $P_c(\theta)$ of observing an induced catastrophe, $P_z(\theta)$ of a zippering event and $P_x(\theta)$ of a crossover when the collision occurs at a relative angle θ. An individual segment of a MT can be either in the growing $(+)$ or shrinking $(-)$ state, provided it is the final segment, and otherwise is in the *inactive* state (0). The main ingredients of the model are graphically summarized in Figure 1.

A coarse-grained description is employed for the alignment of MTs in the cortical array: Instead of individual MTs, local densities of MT segments are considered. The system is assumed to be spatially homogeneous and has as fundamental variables the areal number densities

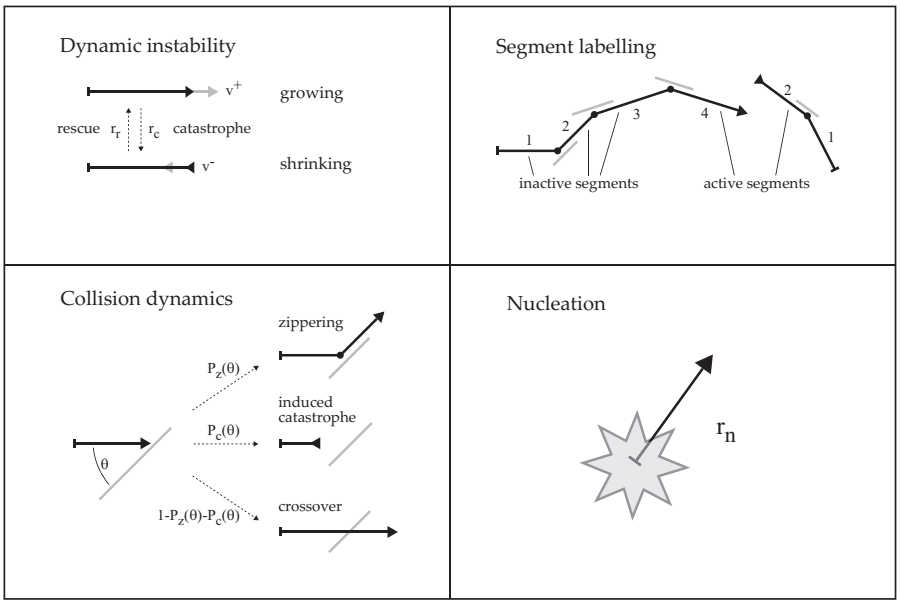

Figure 1. Schematic illustration of the main ingredients of our model for cortical MT dynamics. Top left: The dynamical instability mechanism, with random switches between a growing and a shrinking state. Top right: Labelling of MT segments from the nucleation point (bar),increasing after each zippering event (collision with gray obstructing MT). Bottom left: Collision outcomes. Bottom right: Nucleation of new MTs.

$m_i^\sigma(l,\theta,t)$ of segments in state $\sigma \in \{0,+,-\}$, where the segment number i keeps track of the number of orientation-changing zippering events $(= i-1)$ that preceded in creating the segments, l is the length of the segments and θ their orientation and t the time. These densities obey a set of partial differential evolution equations determined by the overall rates of growth and shrinkage, spontaneous and induced catastrophes, zippering and reactivation of inactive segments through shrinking.

In steady state, the length of all segments, independently of type, turns out to be distributed exponentially with a common average segment length $l(\theta)$

$$m_i^\sigma(l,\theta) = m_i^\sigma(\theta) e^{-l/l(\theta)}, \tag{1}$$

which introduces the angle dependent density at zero length $m_i^\sigma(\theta)$. The stationarity of the total length of MTs implies the balance equation

$$v^+ m_i^+(l,\theta) = v^- m_i^-(l,\theta). \tag{2}$$

An important role is played by the total length density $k(\theta)$ of all MT segments in direction θ, which is defined as

$$k(\theta) = \sum_{i=1}^{\infty} \int dl \; l \; [m_i^+(l,\theta) + m_i^-(l,\theta) + m_i^0(l,\theta)]. \tag{3}$$

Next, the quantities $Q_i(\theta)$, are defined as the ratio between the densities of inactive and active MTs for segments with index i

$$Q_i(\theta) = \frac{m_i^0(\theta)}{m_i^+(\theta) + m_i^-(\theta)}. \tag{4}$$

As is shown in [10], these quantities do not in fact depend on the index i, hence $Q_i(\theta) = Q(\theta)$. Finally, the quantity $t(\theta)$ is defined as the overall density of active segments

$$\begin{aligned} t(\theta) &= \sum_{i=1}^{\infty} \int_0^{\infty} dl \, [m_i^+(l,\theta) + m_i^-(l,\theta)] \\ &= l(\theta) \sum_{i=1}^{\infty} [m_i^+(\theta) + m_i^-(\theta)], \end{aligned} \tag{5}$$

where the second equality is a result of the exponential distribution equation Eq. (1).

We now formulate the governing equations of the system. The "cross-section"of the collisions is determined in part by the geometrical factor $\sin(\theta - \theta')$, where θ is the angle of the incoming growing MT segment and θ' is the angle of the MT "scatterer" with respect to a fixed reference frame. This factor is absorbed into the interaction probabilities by defining

$$f(\theta - \theta') \equiv |\sin(\theta - \theta')| P_f(\theta - \theta')$$

where $f \in \{c, z, x\}$, with c denoting induced catastrophes, z zippering events and x crossovers. We will assume that the collisions are insensitive to the relative orientation of the MT plus-minus end polarities, so that $f(\theta) = f(\pi - \theta)$ for $f \in \{c, z, x\}$. The average segment length $l(\theta)$ is shown to satisfy

$$\frac{1}{l(\theta)} = -g + \int d\theta' [c(\theta - \theta') + z(\theta - \theta')] k(\theta') \tag{6}$$

where

$$g = \frac{r_r}{v^-} - \frac{r_c}{v^+}$$

is called the growth parameter, and characterizes the behavior of the non interacting system. Here we will limit ourselves to the case $g < 0$,

which ensures *a priori* that the length of the MTs remains intrinsically bounded. While the second term on the right-hand side of Eq. (6) could in principle offset the effect of $g > 0$, the resulting system is expected to be absolutely unstable with respect to alignment [10] which would lead to a degenerate non-steady state with continuously elongating MTs. Although the dynamical parameters measured in some plant systems (see e.g. [7]) would suggest that g may be positive, the situation *in planta* is complicated by the activity of the MT severing protein Katanin (see e.g. [17]), which provides an additional channel for MT length control. The effects of the latter, as well as other factors such length capping due to the presence of cell boundaries, are beyond the scope of the present work. For a more extended discussion of these issues please refer to [18].

Using the Eqs. (1) through (5) we find that the length density $k(\theta)$ obeys

$$k(\theta) = l(\theta)[1 + Q(\theta)]t(\theta) \tag{7}$$

The inactive/active ratio $Q(\theta)$ satisfies the following self-consistency equation

$$Q(\theta) = \int d\theta' z(\theta - \theta')k(\theta')l(\theta') \left(1 + Q(\theta')\right). \tag{8}$$

Finally, the overall density of active tip segments $t(\theta)$ obeys

$$t(\theta) = (1 + \frac{v^+}{v^-})l(\theta)m_1^+(\theta) + l(\theta)k(\theta) \int d\theta' z(\theta - \theta')t(\theta'). \tag{9}$$

We see that the density $m_1^+(\theta)$ of zero-length segments that have not been created by a zippering event only appears explicitly in Eq. (9) for the density of active tips. This density is determined by the rate and the orientation at which new MTs are nucleated, which serves as a boundary condition to the steady state equations

$$v^+ m_1^+(\theta) = r_n(\theta). \tag{10}$$

The precise form of the angle-dependent *nucleation rate* $r_n(\theta)$ per unit area, which hitherto was considered to be an isotropic constant, will be discussed below.

2.2. Binding equilibrium of the nucleation complexes

While in the initial stages of cortical array formation almost all of the MT nucleations occur on random locations in the cortex and in random directions, it appears that with increasing array density most of the nucleations are localized to existing MTs [13, 14]. Moreover, these MT-bound nucleations occur with a distinct distribution of orientations

with respect to the parent MT. The majority of all these nucleations is due to the presence of specific nucleation complexes, so-called γ-TuRCs, that are able to bind specifically to MTs, with the precise geometry of the individual binding configurations giving rise to the observed angular pattern of the MT-bound nucleations. To include these effects into our model, we first of all assume that there is finite density of available nucleation complexes. Next, we assume that binding and unbinding happens on a time scale fast compared to the other processes. These assumptions allow us to model the fraction of bound- versus unbound nucleation complexes as being determined by a binding equilibrium.

We let nucleation complexes bind to a unit of length of MT per unit of system area with a rate r_b. In steady state, the length density of MTs is given by (cf. Eq. (3))

$$k_{tot} = \int_0^{2\pi} d\theta\, k(\theta). \tag{11}$$

Bound nucleation complexes can unbind from their parent MT with rate r_u. The overall (areal) density of nucleation complexes is given by $n_{tot} = n_b + n_u$, where n_b and n_u are the bound- and unbound densities respectively. With these definitions, the chemical equilibrium condition then reads

$$n_b r_u = r_b k_{tot} n_u \tag{12}$$

Thus, the fractions of bound and unbound nucleation complexes are given by

$$\begin{aligned} x_b &= \frac{n_b}{n_{tot}} = \frac{r_b k_{tot}}{r_b k_{tot} + r_u} \equiv \frac{k_{tot}}{k_{tot} + k_{\frac{1}{2}}} \\ x_u &= \frac{n_u}{n_{tot}} = \frac{r_u}{r_b k_{tot} + r_u} \equiv \frac{k_{\frac{1}{2}}}{k_{tot} + k_{\frac{1}{2}}}, \end{aligned} \tag{13}$$

where the cross-over density $k_{\frac{1}{2}} = \frac{r_u}{r_b}$, which equals the MT length density for which exactly half the nucleation complexes are bound, controls the shift between the regime of MT densities dominated by unbound nucleations and bound ones respectively.

2.3. Anisotropic distribution of nucleation angles

To determine the angle-dependent nucleation rate $r_n(\theta)$ we now differentiate between nucleations occurring from unbound nucleation complexes and bound ones. Consistent with observations, we take the nucleations from the unbound complexes to be isotropically distributed and assume that an available unbound complex "fires" with a rate

r_n^u. The distribution of nucleation angles in the global reference frame associated with unbound nucleations is trivially given by

$$\psi_u(\theta) = \frac{1}{2\pi}. \tag{14}$$

Nucleations from MT-bound complexes, on the other hand, have been shown to occur with a distinct orientational pattern with respect to the parent MT. We describe this pattern through the normalized *relative nucleation angle distribution* $\nu(\Delta\theta)$, with

$$\int_0^{2\pi} d\Delta\theta\, \nu(\Delta\theta) = 1. \tag{15}$$

To determine the distribution of nucleation angles due to the bound nucleations in the global reference frame, this distribution must be convolved with the orientation distribution of the MTs themselves, thus

$$\psi_b(\theta) = \frac{1}{k_{tot}} \int_0^{2\pi} d\theta' \nu(\theta - \theta') k(\theta'), \tag{16}$$

which as one checks is again normalised. Finally, we take the firing rate of bound nucleation complexes to be r_n^b. In the following, the only condition we will assume on the relative nucleation angle distribution is that it is mirror symmetric with respect to the parent-MT axis, i.e. $\nu(\Delta\theta) = \nu(-\Delta\theta)$.

With these ingredients we can now construct the overall angle-dependent nucleation rate

$$r_n(\theta) = n_u r_n^u \psi_u(\theta) + n_b r_n^b \psi_b(\theta), \tag{17}$$

where n_u and n_b are the densities of unbound and bound nucleation complexes respectively, as derived in the previous section. We graphically illustrate the elements in the construction of the angle-dependent nucleation rate in Figure 2.

It is now convenient to introduce the *overall nucleation rate*

$$r_n = n_b r_n^b + n_u r_n^u, \tag{18}$$

and the *relative firing rate*

$$\rho = \frac{r_n^b}{r_n^u}, \tag{19}$$

and to define

$$r_n(\theta) = \frac{r_n}{2\pi} R(\theta) \tag{20}$$

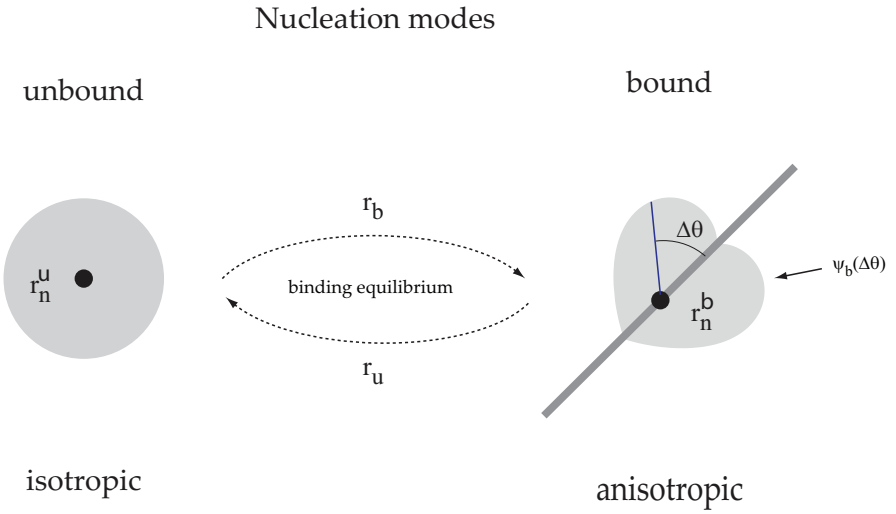

Figure 2. Schematic illustration of the model for the overall angle-dependent nucleation rate, consisting of a chemical equilibrium between isotropic nucleation from unbound nucleation complexes (left) and anisotropic nucleation from microtubule-bound nucleation complexes (right). The light gray shape surrounding the nucleation complex (solid circle) represents a polar plot of the distribution of relative nucleation angles, circular (= isotropic) in the unbound case (left) and a nontrivial function $\psi_b(\Delta\theta)$ in the bound case (right).

which introduces the *absolute nucleation angle distribution* $R(\theta)$. The latter is explicitly given by

$$R(\theta) = \frac{\rho k_{tot}}{\rho k_{tot} + k_{\frac{1}{2}}} 2\pi\psi_b(\theta) + \frac{k_{\frac{1}{2}}}{\rho k_{tot} + k_{\frac{1}{2}}}, \tag{21}$$

where we have used the results of Eq. (13). The choice of the normalization

$$\frac{1}{2\pi}\int_0^{2\pi} d\theta\, R(\theta) = 1 \tag{22}$$

for this distribution serves to minimize the number of explicit factors 2π appearing in the final set of dimensionless equations discussed below.

2.4. Dimensional analysis

The set of equations Eqs. (6)–(9) can be simplified by the use of dimensional analysis. The adoption of the length scale

$$l_0 = \left(\frac{1}{\pi}\frac{v^+}{(1+\frac{v^+}{v^-})r_n/(2\pi)}\right)^{1/3}$$

allows the definition of the dimensionless variables

$$L(\theta) = l(\theta)/l_0, \tag{23}$$
$$K(\theta) = \pi k(\theta) l_0, \tag{24}$$
$$T(\theta) = \pi l_0^2 t(\theta), \tag{25}$$

and dimensionless control parameter of the problem

$$G = g l_0 = \left[\frac{2v^+v^-}{r_n(v^+ + v^-)}\right]^{1/3} \left(\frac{r_r}{v^-} - \frac{r_c}{v^+}\right). \tag{26}$$

It is convenient to adopt the collision operators

$$\mathbf{C}[h](\theta) = \frac{1}{\pi}\int_0^{2\pi} d\theta' c(\theta - \theta')h(\theta'), \mathbf{Z}[h](\theta) = \frac{1}{\pi}\int_0^{2\pi} d\theta' z(\theta - \theta')h(\theta'),$$

where $h(\theta)$ is any integrable function. With these definitions we can formulate the set of dimensionless equations describing the system in the presence of anisotropic nucleation

$$\frac{1}{L(\theta)} = -G + \mathbf{C}[K](\theta) + \mathbf{Z}[K](\theta) \tag{27}$$
$$K(\theta) = L(\theta)(1 + Q(\theta))T(\theta) \tag{28}$$
$$Q(\theta) = \mathbf{Z}[LK(1+Q)](\theta) \tag{29}$$
$$T(\theta) = L(\theta)R(\theta) + L(\theta)K(\theta)\mathbf{Z}[T](\theta) \tag{30}$$

The expression for the absolute nucleation angle distribution is facilitated by the introduction of two additional operators

$$\mathbf{V}[h](\theta) = \frac{1}{\pi}\int_0^{2\pi} d\theta' \nu(\theta - \theta')h(\theta') \tag{31}$$
$$\mathbf{U}[h](\theta) = \frac{1}{\pi}\int_0^{2\pi} d\theta' h(\theta') \tag{32}$$

Non-dimensionalizing the MT length density using the definition in Eq. (24), we find

$$R(\theta) = \frac{2\pi\beta\mathbf{V}[K] + 1}{\beta\mathbf{U}[K] + 1} \tag{33}$$

where the parameter β is given by

$$\beta = \frac{\rho}{k_{\frac{1}{2}} l_0}. \tag{34}$$

Strikingly, this single parameter suffices to capture the relative importance of the bound nucleations with respect to the unbound ones: it is

high whenever the affinity of the nucleation complexes to the MTs is high (small $k_{\frac{1}{2}}$) or when the nucleation rate of the bound complexes is high (large ρ) compared to that of the unbound ones.

3. Results

3.1. Bifurcation analysis

In the isotropic state of the system, all angular dependence drops out and the set of equations becomes

$$\frac{1}{\bar{L}} = -G + (\hat{c}_0 + \hat{z}_0)\bar{K} \tag{35}$$

$$\bar{K} = \bar{L}(1 + \bar{Q})\bar{T} \tag{36}$$

$$\bar{Q} = \hat{z}_0 \bar{L}\bar{K}(1 + \bar{Q}) \tag{37}$$

$$\bar{T} = \bar{L}\bar{R} + \hat{z}_0 \bar{L}\bar{K}\bar{T} \tag{38}$$

where throughout the overbar denotes quantities of the isotropic phase. Here, as in the following, the coefficients $\hat{c}_n$ and $\hat{z}_n$ are the eigenvalues of the operators $\mathbf{C}$ and $\mathbf{Z}$ respectively, on the basis of the cosines $\cos(n\theta)$

$$\mathbf{C}\left[\cos(n\theta)\right] = \hat{c}_n \cos(n\theta), \qquad \mathbf{Z}\left[\cos(n\theta)\right] = \hat{z}_n \cos(n\theta). \tag{39}$$

Next, equation (33) readily gives

$$\bar{R} = 1 \tag{40}$$

showing that the equations for the isotropic state are, as expected, independent of the angular details of the nucleation mechanism and therefore the same as those considered in [10] (cf. Eqs. (40) in that reference).

Using straightforward elimination we can derive the equations

$$\bar{K}(\hat{c}_0 \bar{K} - G)^2 = 1 \tag{41}$$

and

$$\bar{N}(1 - \hat{z}_0 \bar{N})^2 G^3 - [(\hat{c}_0 + \hat{z}_0)\bar{N} - 1]^3 = 0 \tag{42}$$

where $\bar{N} = \bar{L}\bar{K}$, that yield to equivalent ways of characterizing the isotropic state as a function of the control parameter G.

In order to perform a bifurcation analysis, probing the stability of the isotropic state against anisotropic perturbations, we parameterize

the solutions to the full problem as

$$L = \bar{L}(1+\lambda) \tag{43}$$
$$K = \bar{K}(1+\kappa) \tag{44}$$
$$Q = \bar{Q}(1+\chi) \tag{45}$$
$$T = \bar{T}(1+\tau) \tag{46}$$

where we assume that the perturbations λ, κ, χ and τ are small. Inserting into the equations (27), (28), (29) and (30) and expanding to the first order in the perturbations we obtain

$$-\lambda = \bar{N}\left(\mathbf{C}[\kappa] + \mathbf{Z}[\kappa]\right) \tag{47}$$
$$\kappa = \lambda + \tau + \hat{z}_0\bar{N}\chi \tag{48}$$
$$\chi = \frac{1}{\hat{z}_0}\mathbf{Z}\left[\kappa + \lambda + \hat{z}_0\bar{N}\chi\right] \tag{49}$$
$$\tau = \lambda + \bar{N}\left(\hat{z}_0\kappa + \mathbf{Z}[\tau]\right) + (1 - \hat{z}_0\bar{N})\mathbf{B}[\kappa] \tag{50}$$

where

$$\mathbf{B}[\kappa] = \frac{\beta\bar{K}}{2\beta\bar{K}+1}\left(2\pi\mathbf{V}[\kappa] - \mathbf{U}[\kappa]\right) \tag{51}$$

Eliminating λ, χ and τ from these equations we find a linear eigenvalue problem for the length density perturbation κ

$$(1 - \hat{z}_0\bar{N})\kappa = -2\bar{N}\mathbf{C}[\kappa] + (1 - \hat{z}_0\bar{N})\mathbf{B}[\kappa] \tag{52}$$

which is satisfied whenever $\kappa(\theta)$ is an eigenfunction of both the operators $\mathbf{C}$ and $\mathbf{B}$. Given the symmetries of the operators $\mathbf{C}, \mathbf{V}$ and $\mathbf{U}$ the relevant set of common eigenfunctions is the family $\cos(2j\theta)$, where $j \geq 1$ ($j = 0$ is not an anisotropic perturbation). We assume, as in [10], that the longest wavelength perturbation $\cos(2\theta)$, i.e. the case $j = 1$, corresponds to the first break of symmetry on increasing G. Inserting this assumption into the eigenvalue equation (52), we get the equation which implicitly defines the location of the corresponding bifurcation point

$$(1 - \hat{z}_0\bar{N}) = -2\bar{N}\hat{c}_2 + (1 - \hat{z}_0\bar{N})\frac{2\beta\bar{K}}{2\beta\bar{K}+1}\nu_2. \tag{53}$$

Here we have introduced the *co-alignment parameter*

$$\nu_2 = \int_0^{2\pi} d\theta \cos(2\theta)\nu(\theta) \in [-1, 1], \tag{54}$$

which provides the relevant measure for the degree of orientational co-alignment of MTs originating from bound nucleation events with their

parent MTs. Its appearance in the bifurcation equation (53) provides an *a posteriori* theoretical underpinning for its heuristic use in the analysis of the simulation data in Ref. [15]. When $\nu_2 = 1$, which occurs e.g. when $\nu(\theta) = \delta(\theta)$), the nucleated MTs are perfectly co-aligned (either in the plus- or minus end direction) with the parent MT, when $\nu_2 = -1$, which occurs when $\nu(\theta) = \frac{1}{2}\left(\delta\left(\theta - \frac{\pi}{2}\right) + \delta\left(\theta + \frac{\pi}{2}\right)\right)$, the nucleated MTs are maximally dis-aligned (= perpendicular) to the parent MT. Finally, the intermediate case $\nu_2 = 0$ occurs when the MTs are either nucleated evenly into the "neutral" directions $\pm\frac{\pi}{4}$ and $\pm\frac{3\pi}{4}$ or simply isotropically $\left(\nu(\theta) = \frac{1}{2\pi}\right)$.

The bifurcation equation (53), together with the isotropic state equations (41) and (42), allow us to calculate the critical value of the control parameter G_* at which the bifurcation occurs. We start by rewriting Eq. (53) as

$$\bar{N} = \frac{1}{\hat{z}_0 + \bar{M}}, \tag{55}$$

where

$$\bar{M} = (-2\hat{c}_2)\,\frac{(2\beta\bar{K}+1)}{\left(2\beta\bar{K}(1-\nu_2)+1\right)}. \tag{56}$$

Inserting this form of $\bar{N}$ into Eq. (42), we obtain

$$G_* = \bar{M}^{1/3}\left(\frac{\hat{c}_0}{\bar{M}} - 1\right). \tag{57}$$

We note that this result is valid *independent* of the sign of G_*. However, in line with our choice, discussed in Sect. 2.1, to limit the analysis to the regime $G < 0$, so that we are ensured an ordered steady-state can exist, we now enquire under which constraints in fact $G_* < 0$. As by definition $\hat{c}_0 > 0$, we should need both $\bar{M} > 0$ as well as $\bar{M} > \hat{c}_0$. We now note that $\operatorname{sgn}\left(\bar{M}\right) = -\operatorname{sgn}\left(\hat{c}_2\right)$, so that we require $\hat{c}_2 < 0$. As discussed in [10], this is generically the case for induced catastrophe probabilities $P_c(\theta)$ that are (semi)monotonically increasing in θ on the interval $\left[0, \frac{\pi}{2}\right]$, which in turn is consistent with the in vivo observations [6]. Next, we note that for $\nu_2 \in [0,1]$, i.e. the range of nucleations that are effectively in the forward to neutral directions with respect to the parent MTs, $\bar{M} \geq (-2\hat{c}_2)$, so that it is then sufficient to require, as in [10], that $(-2\hat{c}_2) > \hat{c}_0$. The latter requirement is readily met for realistic induced catastrophe probability profiles. Finally, the available data indicates that $\nu_2 \sim 0.7 - 0.9.$, i.e. in the required regime [13, 14]. In the following we therefore freely adopt these constraints.

We also note that in the limit $\beta = 0$, where the nucleation complexes do not bind to the MTs and all nucleations take place isotropically in

the bulk, Eq. (57) correctly reduces to

$$G_*^{(0)} = (-2\hat{c}_2)^{1/3}\left(\frac{\hat{c}_0}{-2\hat{c}_2} - 1\right), \tag{58}$$

the result previously obtained in [10]. After some algebra, we can also obtain the first order effect of a non-zero ν_2 on the location of the transition

$$G_*^{(1)} = \left.\frac{\partial G_*}{\partial \nu_2}\right|_{\nu_2=0} = \frac{1}{3\hat{c}_2}\left(-2\hat{c}_2\right)^{\frac{1}{3}}(\hat{c}_0 - \hat{c}_2)\frac{2\beta\bar{K}_*^{(0)}}{(2\beta\bar{K}_*^{(0)}+1)} < 0 \tag{59}$$

where $\bar{K}_*^{(0)}$ is the critical length density at $\nu_2 = 0$. This result indicates that for positive co-alignment ($\nu_2 > 0$) the bifurcation point is shifted towards lower G values, indicating a widening of the ordered region. Note also that Eq. (57) implies that, in spite of the anisotropic nucleation mechanism, the location of the transition does not depend on the presence or absence of the zippering mechanism, in line with the analysis presented in [10].

To obtain the bifurcation point for arbitrary values of ν_2, we introduce (57) into the equation (41) coupling $\bar{K}$ and G in the isotropic state, ultimately obtaining a 15th order polynomial equation in $\sqrt{\bar{K}}$ (not shown). Numerical solutions of this equation allow us to identify the unique positive real root that yields the critical value of the MT length density $\bar{K}_*$, which in turn can be used in Eq. (41) to back out the critical value G_* of the control parameter. The results of this procedure are discussed in the next section.

3.2. Numerical solutions

To present our numerical results on the location of the ordering transition we first have to choose a set of collision probabilities. Following Refs. [7] and [9] we opted for the following stylized representation of the available data

$$\begin{aligned} P_z(\Delta\theta) &= \begin{cases} 1 & \Delta\theta < \theta_c = 40^\circ \\ 0 & \theta_c \le \Delta\theta \le 90^\circ \end{cases} \\ P_c(\Delta\theta) &= \begin{cases} 0 & \Delta\theta < \theta_c = 40^\circ \\ p_c & \theta_c \le \Delta\theta \le 90^\circ \end{cases} \end{aligned} \tag{60}$$

In Figure 3 we show the result for the critical value G_* as a function of ν_2 for a few values of the parameter β in the specific case $p_c = 0.5$.

We see that for all values of the parameter β, which governs the strength of the anisotropic nucleation mechanism, the critical value

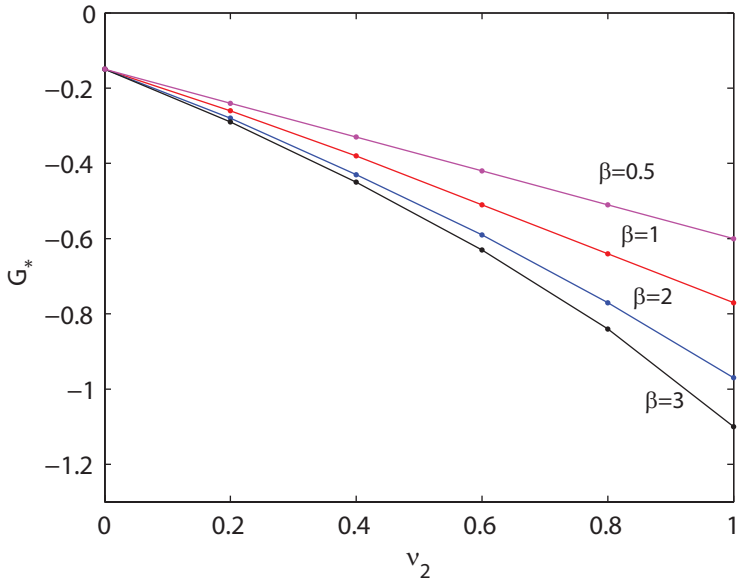

Figure 3. Critical values G_* of the control parameter G as a function of the degree of co-aligned nucleation ν_2 for 4 different values of the parameter β.

of the control parameter is a decreasing function of the coalignment parameter ν_2. This means that the regime of MT dynamical parameter for which the system establishes an ordered state is widened. Indeed, we can interpret the co-aligned nucleation of new MTs as an additional positive feedback mechanism on the basic "survival of the aligned" mechanism presented in [10]: longer-lived aligned MTs also generate "offspring" that is similarly aligned, will therefore experience fewer catastrophe inducing collisions, and hence "inherit" the longevity of their parents.

3.3. Comparison to simulations

In order to verify that the results of our mean-field theory are reasonable, we here compare them with results from particle-based simulations. These employed a MT-bound nucleation distribution with $n\%$ of nucleation along the parent MT in the forward direction, and the remainder isotropically distributed. By varying the percentage n, the degree of co-alignment, which in this case is simply given by $\nu_2 = n/100$, can be varied over the full range $[0, 1]$. For details of the simulation, including the technique to infer the critical control parameter from the simulation data on the second-rank order parameter S_2 as a function of the control parameter G, please refer to Ref. [15].

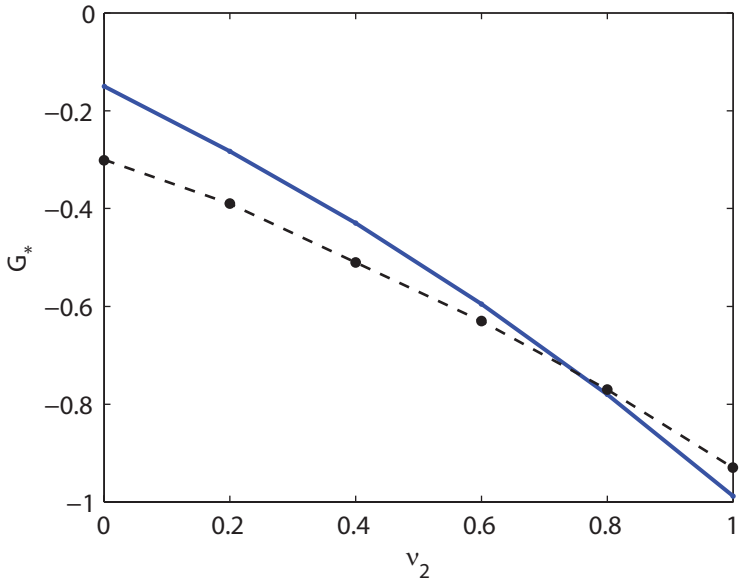

Figure 4. Comparison between simulation results of Ref. [15] (filled circles, dashed line to guide the eye) and theoretical predictions (solid line) for the critical values G_* of the control parameter as a function of the degree of co-aligned nucleation ν_2 for a model with $p_c = 0.5$.

In spite of the fact that the simulation employed the so-called simple bundle collision dynamics, in which an MT impinging on a bundle only sees a single target MT [19], and had explicitly treadmilling MTs [20], the qualitative agreement between the predicted locations of the transitions and the ones observed in the simulations is satisfactory (see Figure 4), specifically in reproducing the marked widening of the ordered region.

4. Conclusion

We have shown that the theoretical framework for describing the self-organisation of the microtubule cortical cytoskeleton in plant cells first presented in [10] can be robustly extended to include the biologically relevant MT-bound anisotropic nucleations. The relative importance of this effect as compared to the background isotropic nucleation events is predicted to depend on a single dimensionless number β, that takes into account both the affinity of nucleation complexes for MTs, as well as a possible binding-state dependence of their firing rate. Our bifurcation analysis furthermore reveals that averaged co-alignment of the bound

nucleations with the parent MT, captured by the parameter ν_2, is the main determinant of the location of the transition. The significant widening of the ordered regime with increasing ν_2 can be ascribed to a positive feedback mechanism that enhances the "survival of the aligned" mechanism already described in [8]: aligned MTs "beget" co-aligned "offspring" thus increasing the survival of the preferential direction. Finally, the comparisons with the particle-based simulations, show that the theory, albeit of a mean-field nature, is a robust approximation to full dynamical system including the spatial dependencies.

The work described here is a first step in the extension of the model to include a number of factors that are known to be involved in the *in vivo* ordering process. Here, we specifically mention the effects of minus-end treadmilling, MT severing by Katanin-like proteins and finiteness of the available tubulin monomer pool. Including these effects is part of our ongoing research effort.

Acknowledgements

This work is part of the research programme of the Foundation for Fundamental Research on Matter (FOM), which is part of the Netherlands Organisation for Scientific Research (NWO).

References

1. Sidney L. Shaw, Jacques Dumais, and Sharon R. Long. Cell surface expansion in polarly growing root hairs of medicago truncatula. *Plant Physiology*, 124(3):959–970, 2000.
2. David W. Ehrhardt and Sidney L. Shaw. Microtubule dynamics and organization in the plant cortical array. *Ann. Rev. of Plant Biol.*, 57:859–875, 2006.
3. Alexander R. Paredez, Christopher R. Somerville, and David W. Ehrhardt. Visualization of cellulose synthase demonstrates functional association with microtubules. *Science*, 312(5779):1491–1495, 2006.
4. Ryan Gutierrez, Jelmer J. Lindeboom, Alex R. Paredez, Anne Mie C. Emons, and David W. Ehrhardt. Arabidopsis cortical microtubules position cellulose synthase delivery to the plasma membrane and interact with cellulose synthase trafficking compartments. *Nature Cell Biol.*, 11:797–806, 2009.
5. A. Desai and T. J. Mitchison. Microtubule polymerization dynamics. *Annu. Rev. Cell Dev. Biol.*, 13:83–117, 199.
6. R. Dixit and R. Cyr. Encounters between dynamic cortical microtubules promote ordering of the cortical array through angle-dependent modifications of microtubule behavior. *Plant Cell*, 16:3274–3284, 2004.

7. J.F. Allard, G.O. Wasteneys, and E.N. Cytrynbaum. Mechanisms of self-organization of cortical microtubules in plants revealed by computational simulations. *Mol. Biol. Cell*, 21:278–286, 2010.
8. S.H. Tindemans, R.J. Hawkins, and B.M. Mulder. Survival of the aligned:ordering of the plant cortical microtubule array. *Phys. Rev. Lett.*, 104:058103, 2010.
9. E.C. Eren, R. Dixit, and N. Gautam. A 3d computer simulation model reveals the mechanisms for self-organization of plant cortical microtubules into oblique arrays. *Mol. Biol. Cell*, 21:2674–2684, 2010.
10. R.J. Hawkins, S.H. Tindemans, and B.M. Mulder. Model for the orientational ordering of the plant microtubule cortical array. *Phys. Rev. E*, 82:011911, 2010.
11. Jens Luders and Tim Stearns. Microtubule-organizing centres: a re-evaluation. *Nature Rev. Mol. Cell Biol.*, 8:161–167, 2007.
12. T. Murata, S. Sonobe, T.I. Baskin, S. Hyodo, S. Hasezawa, T. Nagata, T. Horio, and M. Hasebe. Microtubule-dependent microtubule nucleation based on recruitment of big gamma-tubulin in higher plants. *Nature Cell Biol.*, 7:961–968, 2005.
13. J. Chan, A. Sambade, G. Calder, and C. Lloyd. Arabidopsis cortical microtubules are initiated along, as well as branching from, existing microtubules. *Plant Cell*, 21:2298–2306, 2009.
14. Nakamura M., Ehrhardt D.W., and Hashimoto T. Microtubule and katanin-dependent dynamics of microtubule nucleation complexes in the acentrosomal arabidopsis cortical array. *Nature Cell Biol.*, 12:1064–1070, 2010.
15. E.E. Deinum, S.H. Tindemans, and B.M. Mulder. Taking directions: The role of microtubule-bound nucleation in the self-organization of the plant cortical array. *Phys. Biol.*, 8:056002, 2011.
16. M. Dogterom and S. Leibler. Physical aspects of the growth and regulation of microtubule structures. *Phys. Rev. Lett.*, 70:1347–1350, 1993.
17. David H. Burk, Ruiqin Zhong, and Zheng-Hua Ye. The katanin microtubule severing protein in plants. *Journal of Integrative Plant Biology*, 49(8):1174–1182, 2007.
18. Eva E Deinum and Bela M Mulder. Modelling the role of microtubules in plant cell morphology. *Current Opinion in Plant Biology*, 16(6):688 – 692, 2013.
19. S. H. Tindemans. *Biomolecular design elements : cortical microtubules and DNA-coated colloids*. PhD thesis, Wageningen University, 2009.
20. Clare M. Waterman-Storer and E.D. Salmon. Microtubule dynamics: Treadmilling comes around again. *Current biol.*, 7:R369–R372, 1997.